ChemPhysChem
Research Article
doi.org/10.1002/cphc.202200775
Chemistry Europe
European Chemical Societies Publishing

www.chemphyschem.org

Revealing the Chemical State of Palladium in Operating In_2O_3 Gas Sensors: Metallic Pd Enhances Sensing Response and Intermetallic In_xPd_y Compound Blocks It

Oleksandr Ovsianytskyi,[a] Maged F. Bekheet,[a] Albert Gili,[a, b] and Aleksander Gurlo*[a]

The sensing response of metal oxides activated with noble metal nanoparticles is significantly influenced by changes to the chemical state of corresponding elements under operating conditions. Here, a PdO/rh-In_2O_3 consisting of PdO nanoparticles loaded onto rhombohedral In_2O_3 was studied as a gas sensor for H_2 gas (100–40000 ppm in an oxygen-free atmosphere) in the temperature range of 25–450 °C. The phase composition and chemical state of elements were examined by resistance measurements combined with synchrotron-based in situ X-ray diffraction and ex situ X-ray photoelectron spectroscopy. As found, PdO/rh-In_2O_3 undergoes a series of structural and chemical transformations during operation: from PdO to Pd/PdH_x and finally to the intermetallic In_xPd_y phase. The maximal sensing response (R_{N2}/R_{H2}) of $\sim 5 \cdot 10^7$ towards 40000 ppm (4 vol %) H_2 at 70 °C is correlated with the formation of $PdH_{0.706}$/Pd. The In_xPd_y intermetallic compounds formed around 250 °C significantly decrease the sensing response.

Introduction

Hydrogen gas is considered to be a solution for future energy supply. It is an odorless, colorless, and highly explosive gas that is often stored at very high pressures and can be very dangerous if leaks occur during storage or application. Thus, it is crucial to quickly detect any leakage of hydrogen to avoid any danger of explosion. Resistive gas sensors based on semiconducting metal oxides, such as SnO_2,[1] ZnO,[2] WO_3,[3] TiO_2,[4] and In_2O_3[5] change their resistance according to the changes in hydrogen gas concentration representing cheap technology for hydrogen detection. The drawback is due to the high operating temperatures of sensors, typically above 200 °C. The sensing response of metal oxide sensors to hydrogen is significantly improved upon their "activation" with small amounts of noble metals such as Pd,[6,7] Pt,[6] Ag,[8] and Au.[8] Moreover, this also results in a decrease of the operating temperatures of the sensors down to room temperature.[9] Despite long-lasting research towards exploring the mechanism of hydrogen detection on noble metal (and especially, palladium) activated metal oxides, there is still a significant controversy concerning this question. The mechanisms discussed in the literature include spill-over effect, Fermi-level control, catalytic enhancement, and single-atom effects (see, for example, overview in the Ref. [10]). However, possible structural transformations neither in metallic particles nor those appearing due to the chemical reactions with metal oxide itself under operating conditions have not been discussed so far. Since they can be masked in oxygen-containing atmospheres mainly due to fast oxidation reactions, we decided to address this issue in an oxygen-free atmosphere on a model system purposefully designed for that study.

We focus on the hydrogen detection mechanism with PdO loaded on metastable rhombohedral (corundum-type) In_2O_3 (rh-In_2O_3[11]). Our previous in situ synchrotron X-ray diffraction studies showed that 5 wt % PdO-loaded rh-In_2O_3 undergoes a sequence of phase transformations upon heating under a pure H_2 atmosphere.[12] The PdO is first reduced to Pd metal at ~30 °C, followed by the formation of $PdH_{0.706}$ hydride and, subsequently, of intermetallic compounds (IMCs) such as InPd (at 230 °C) and In_3Pd_2 (at 300 °C). Due to these prompt and proven phase transformations, which are observable at the sensor's operating temperatures between 25 and 400 °C, PdO/rh-In_2O_3 represents a unique model system for answering the aforementioned questions about the mechanism of hydrogen detection.

Accordingly, in the present study, we apply complementary sensing tests (resistance measurements) with in situ synchrotron X-ray diffraction and ex situ X-ray photoelectron spectroscopy. These methods allow us to correlate the H_2 sensing properties of the specimens with the structure and oxidation state of Pd-containing phases.

---

[a] *O. Ovsianytskyi, Dr.-Ing. M. F. Bekheet, Dr.-Ing. A. Gili, Prof. Dr. A. Gurlo*
Fachgebiet Keramische Werkstoffe / Chair of Advanced Ceramic Materials,
Institut für Werkstoffwissenschaften und -technologien
Technische Universität Berlin
Straße des 17. Juni 135, 10623 Berlin, Germany
E-mail: gurlo@ceramics.tu-berlin.de
Homepage: www.tu.berlin/ceramics
[b] *Dr.-Ing. A. Gili*
current address, PVcomB
Helmholtz-Zentrum Berlin für Materialien und Energie
Schwarzschildstr. 3, 12489 Berlin, Germany

Supporting information for this article is available on the WWW under https://doi.org/10.1002/cphc.202200775

Results and Discussion

Figure 1 displays the sensor signals (i.e., resistance ratio R_{N2}/R_{H2}) of the PdO/rh-In_2O_3 and pure rh-In_2O_3 sensors sample towards 100 ppm and 40000 ppm H_2 gas (i.e. the lowest and the highest concentrations used in this experiment) in the temperature range of 25–450 °C. Remarkably, the PdO/rh-In_2O_3 sample possesses enormously large sensors signals at temperatures below 250 °C; the sensor signal increases starting from 25 °C and reaches its maximum at 70 °C, and then it slightly decreases in the temperature range from 100 °C to 250 °C, before a rapid decrease in temperatures above 250 °C. In contrast, the rh-In_2O_3 sensor starts to show some noticeable response towards H_2 gas only at temperatures greater than 100 °C. Later, its response increases with temperature, reaching the maximum value at 250 °C, and at temperatures above 250 °C, the response starts to decline rapidly. Moreover, PdO/rh-In_2O_3 sensor is highly sensitive to low hydrogen concentrations (Figure 2) and is also able to detect even much lower H_2 concentrations around 1 ppm (Figure S1) which rh-In_2O_3 does not recognize. However, as displayed in Figure 2 and S2–3, starting from 100 °C the PdO/rh-In_2O_3, in contrast to rh-In_2O_3, is becoming saturated, meaning that after an initial large sensor decrease in 100 ppm H_2 no further resistance change in higher hydrogen concentrations is observed.

To clarify the reason for this remarkable difference in gas-sensing properties of both materials as well as to understand the influence of the temperature, we designed and conducted a series of experiments that include in situ X-ray diffraction in the simulated gas conditions similar to the gas sensing tests, stabilization of selected Pd-containing phases and gas sensing test with these compositions and characterization of Pd oxidation states with X-ray photoelectron spectroscopy.

Rietveld refinement analysis of high-resolution synchrotron X-ray diffraction data collected at room temperature (Figure S4a) on the initial (starting) PdO/rh-In_2O_3 sample reveals that the sample contains 94.9 ± 1 wt% rh-In_2O_3, 5.0 ± 0.8 wt% PdO, and ~0.1 ± 0.05 wt% of PdH_x. PdH_x originates from the synthesis procedure of the materials. The *a* and *c* parameters of the rh-In_2O_3 lattice in the sample are 5.4846(5) and 14.5170(1), respectively, which are very close to the reported values for pure rh-In_2O_3,[12] confirming no Pd doping in the rh-In_2O_3 phase. The crystal structure of rh-In_2O_3 and PdO in the initial specimen was further corroborated by the SAED/HAADF/EDX pattern.[12] All reflections were unequivocally assigned to either rh-In_2O_3 or tetragonal PdO.

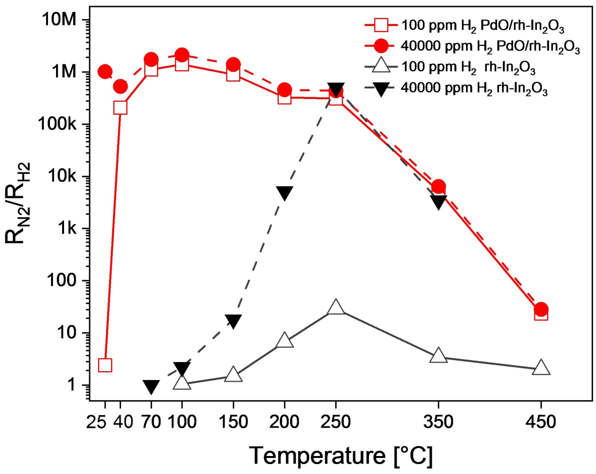

Figure 1. Sensor signals (*i.e.*, R_{N2}/R_{H2}) of PdO/rh-In_2O_3 and pure rh-In_2O_3 sensors towards 100 ppm and 40000 ppm H_2 gas in N_2 at 25–450 °C.

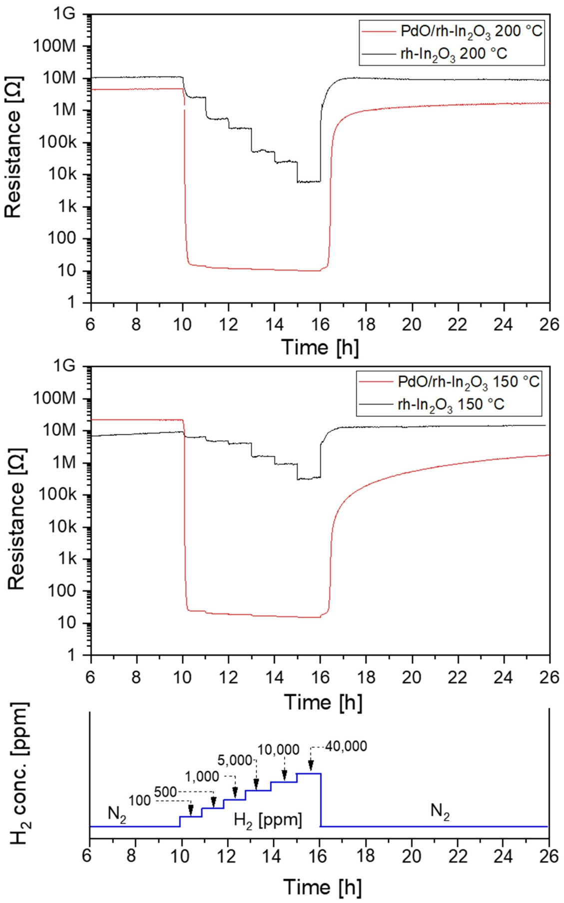

Figure 2. Sensor response of PdO/rh-In_2O_3 and rh-In_2O_3 towards H_2 gas at 150 °C and 200 °C. At the bottom, the profile of hydrogen concentration changes in N_2 is shown.

The morphology and elemental distribution of the PdO/rh-In_2O_3 sensor before and after treatment in 40000 ppm H_2 in N_2 (after the sensing experiments), at 250 °C for 2 hours, were investigated by SEM/EDX. As shown in Figure S4 and elsewhere,[12] the PdO/rh-In_2O_3 powder consists of slightly agglomerated nanosized spherical grains. EDX elemental mapping reveals that the distribution of Pd on the surface of the sample becomes more uniform and homogeneous after treating the sample in H_2 gas at 250 °C, suggesting a change in the chemical composition on the surface of the sample after the gas sensing tests.

Figure 3 (window selected for the more detailed analysis) and Figure S5 (full pattern) show in situ XRD patterns collected during heating of PdO/rh-In_2O_3 powder from 25 °C to 200 °C

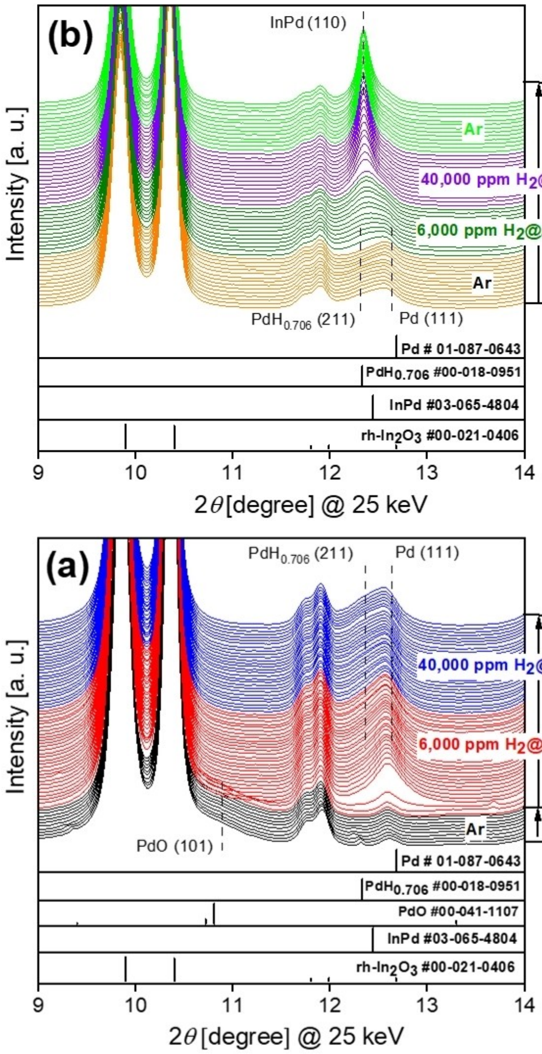

Figure 3. X-ray diffraction patterns (a window between 9 and 14 degree is displayed here, for the full pattern see Figure S5) collected in situ during heating of the PdO/In_2O_3 powder from 25 °C to 200 °C (a) and at 250 °C (b) in the Ar atmosphere, followed by isothermal steps (30 min per step) under two different concentrations of H_2 in the Ar atmosphere (6000 ppm and 40000 ppm H_2).

and 250 °C in the Ar atmosphere, followed by isothermal steps under two different concentrations of H_2 in the Ar atmosphere (6,000 ppm and 40000 ppm H_2). As shown in Figure 3a, all reflections in the XRD pattern of the sensor at room temperature could be assigned to rh-In_2O_3 (PDF-card #00-021-0406) and tetragonal PdO (PDF-card #00-041-1107) phases. Additionally, XRD reflections corresponding to the $PdH_{0.706}$ phase (PDF-card #00-018-0951) are also observed in the pattern at room temperature and have disappeared under heating in the Ar atmosphere at ~170 °C. These results suggest the initial sample might contain a low amount of metallic Pd that adsorbed H_2 at room temperature to form the $PdH_{0.706}$ phase.

In contrast, the PdO phase is stable during the heating step in the Ar atmosphere, even at 200 °C, before transforming into metallic Pd after only 5 min of injecting 6000 ppm H_2 at 200 °C. With further increase in time, a broad XRD reflection attributed to the PdH_x phase appears again, and its intensity increases with time under both concentrations of H_2 in the Ar atmosphere, suggesting the increase in the amount of the PdH_x phase. In contrast, the intensity of this XRD reflection decreases again by purging the sample with pure Ar gas at 250 °C (Figure 3), indicating the decrease in the amount of the PdH_x phase again.

The increase in the amount of the PdH_x phase can be explained by the adsorption and incorporation of hydrogen in the Pd lattice under both H_2 concentrations, while the decrease can be due to the desorption of hydrogen under a pure Ar atmosphere. At 250 °C, the formation of InPd IMC starts at the low concentration of H_2 (6000 ppm H_2) and is completed by increasing the H_2 concentration to 40000 ppm. No further phase transformation takes place at 250 °C even after a holding time of 1 hour. The sequence and temperature of phase transformations are in good agreement with our previous work under the pure H_2 atmosphere.[12] Moreover, Rietveld's refinement of the XRD pattern (Figure S4b) recovered at room temperature after the in situ experiment reveals that the sample contains 90.5 ± 0.5 wt% rh-In_2O_3 and 9.5 ± 0.3 wt% InPd, which agrees with the experimental amount of Pd used in the preparation of the sensor. These results suggest the formation of a stoichiometric InPd phase.

Further Le Bail analysis of in situ XRD data presented in Figure 4 allows us to look deeper into the expansion/contraction of different crystalline phases in our sample, discovering its ability to absorb hydrogen gas. Although the intermetallic InPd phase is crystallized in the cubic structure with space group *Pm*-3*m*, we used the space group *Fm*-3*m* for this phase in the Le Bail fit analysis for better comparison with the parameter of metallic Pd that crystallized in the latter space group.

First, we analyze the Pd lattice parameter *a*, which increases first at 200 °C while flushing the sample with hydrogen gas, meaning that hydrogen absorbs into the lattice and causes its expansion, and after flushing the sample with Ar at 250 °C, the lattice parameter experiences a significant drop due to hydrogen desorption even despite the increasing temperature. However, the same procedure performed at 250 °C doesn't affect the InPd lattice parameter, meaning that almost no hydrogen was absorbed inside a lattice, but rather might be adsorbed on the surface of the sample if we will take into consideration the changes in the InPd weight fraction. On the other hand, we can see how rh-In_2O_3 changes its unit cell volume during increasing the temperature and experiencing hydrogen absorption. We can observe an increase in the unit cell volume during absorption of H_2 gas at 200 °C, then a further increase during flushing with Ar at 250 °C, and then an additional increase after the introduction of H_2 gas at 250 °C, followed by a decrease in the unit cell volume during final flushing with Ar.

The change in the chemical state of palladium during sensor operation was further studied by the XPS. Figure 5 shows the X-ray photoelectronic Pd $3d_{5/2}$, In $3d_{5/2,}$ and O1s spectra of the PdO/rh-In_2O_3 sensor before and after the gas sensing tests at different temperatures. As shown in Figure 5a, the Pd $3d_{5/2}$ peak of the as-prepared PdO/In_2O_3 sample can be fitted with two

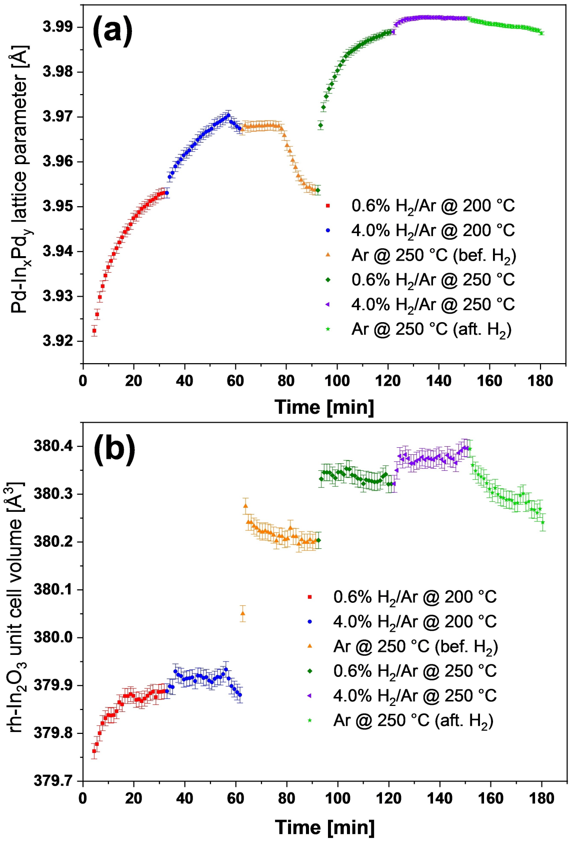

Figure 4. Results of Le Bail fitting of in situ XRD patterns of the PdO-In_2O_3 sample collected during treatment with 6,000 ppm and 40,000 ppm H_2 in the Ar atmosphere at 200 °C and 250 °C (presented in Figure 3) showing (a) the lattice parameter *a* of metallic Pd and intermetallic In_xPd_y phases using the space group *Fm*-3 *m* for all phases for easy comparison and (b) the unit cell volume of rh-In_2O_3 phase.

peaks at 337.2 eV and 335.8 eV, which can be attributed to Pd^{+2} in PdO and Pd^0 in metallic Pd or PdH_x, respectively.[13] These results are in good agreement with XRD results, which revealed the presence of crystalline PdO and PdH_x phases in the sample. Exposure to hydrogen at 150 °C results in the shift of Pd $3d_{5/2}$ peaks to lower binding energies of 335.27 eV and 335.9 eV, suggesting the reduction of PdO into metallic Pd, with higher intensity peaks indicating the presence of PdH_x. At a temperature of 200 °C, the Pd $3d_{5/2}$ peaks are seen to be shifted slightly to higher binding energies, implying the beginning of the alloying process to form In_xPd_y IMC.[14] However, most of the Pd remains in the metallic form at this temperature. The intensity and area of the peak located at 335.9 eV significantly increased together with further shifting towards higher binding energy testing the sample at 250 °C, indicating the further formation of InPd IMC. Our XPS results are in good agreement with those of an in situ XPS study conducted earlier.[15]

According to the XRD and XPS findings described above, the PdO-loaded rh-In_2O_3 sample experiences a series of structural transformations during treatment in an H_2 atmosphere, which might be the reason for the change in the sensor's response to the temperature. The PdO reduced first to Pd metal at ~50 °C, next followed by $PdH_{0.706}$ hydride formation at 70 °C and, subsequently, intermetallic compounds (IMC) formation such as InPd (at 250 °C). This sequence of phase transformations under low concentrations of H_2 (40000 ppm H_2) agrees with that previously observed for pure hydrogen atmosphere.[12] To correlate these changes with the gas sensing properties, a series of model experiments were conducted, as displayed in Figure 6. The gas sensing properties of PdO/rh-In_2O_3 and pure rh-In_2O_3 sensors are studied starting from the 25 °C after the pre-treatment step in the gas sensing conditions (from 100 ppm to 40000 ppm H_2 gas in N_2) at a temperature of 250 °C at which structural phase transformation – i.e., the formation of InPd IMC occurs.

As shown in Figure 6, the optimum sensing temperature point of the PdO/rh-In_2O_3 sensor treated at 250 °C (after the formation of the InPd IMC) has been shifted from 70 °C to 250 °C together with a sharp drop in the sensor signals meaning that the maximum response of the sensor drops on more than 4 orders of magnitude in comparison to the as-prepared PdO/rh-In_2O_3 sensor. In contrast, the rh-In_2O_3 sensor treated at identical conditions shows the same changes in the resistance towards H_2 as in the previous test of the as-prepared pure rh-In_2O_3 powder. These findings suggest that such a huge decline in the sensor's response in the PdO/rh-In_2O_3 system might be due to the formation of the InPd IMC on the surface of the sample with a reduced hydrogen adsorption ability, as confirmed by in situ XRD experiments (Figure 3). To conclude, the maximum response of the PdO/rh-In_2O_3 sensor toward H_2 is observed in the temperature range of 40–100 °C thanks to the transformation of PdO into metallic Pd, and as a result, higher H_2 adsorption capability due to the Pd catalytic activity that facilitates simultaneous dissociation and absorption of hydrogen into the interstitials in the bulk of the metal to form an alpha-hydride phase. Above 100 °C, the H_2 desorption dominates over the adsorption process – resulting in a gradual decline of the sensor's response. The significant decrease in the sensor response above 250 °C might be due to the formation of intermetallic compounds (IMC), such as InPd (at T > 230 °C).[12] Scheme 1 displays the material changes throughout the whole experiment. The mechanism of H_2 sensing in oxygen-

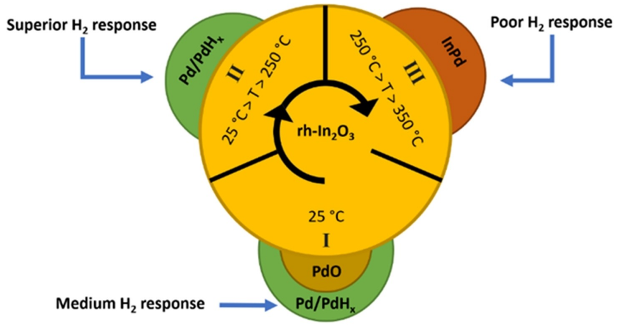

Scheme 1. Schematic illustrations of the structural transformations of the Pd/PdO-loaded rh-In_2O_3 at elevated temperatures in the H_2-containing atmosphere.

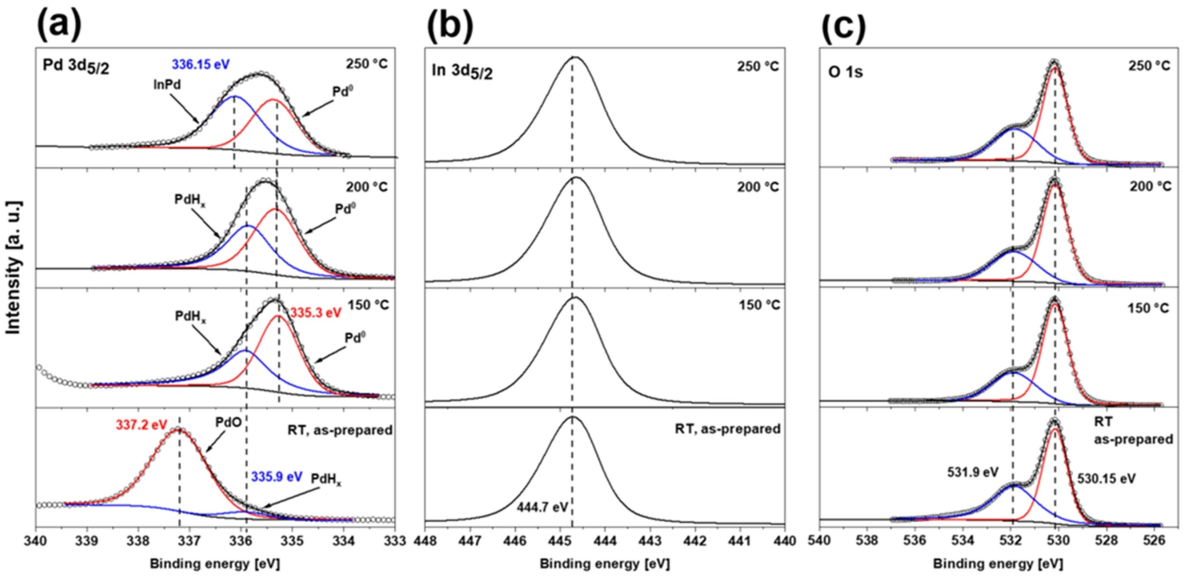

Figure 5. X-ray photoelectronic spectra of the (a) Pd $3d_{5/2}$ region, (b) In $3d_{5/2}$ region, and (c) O 1s region of as-prepared PdO/rh-In_2O_3 sample and after treatment at simulated sensor operating conditions (150–250 °C, 100–40000 ppm H_2 concentration).

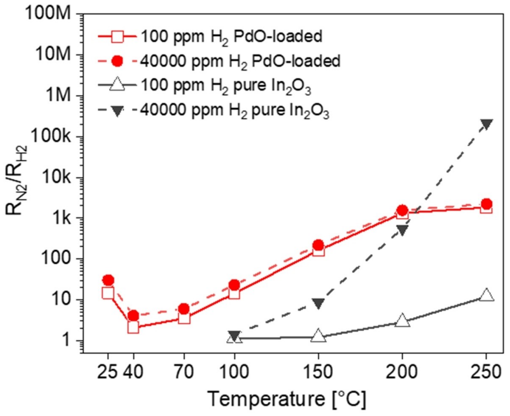

Figure 6. Sensor signals (*i.e.*, R_{N2}/R_{H2}) of PdO/rh-In_2O_3 and pure rh-In_2O_3 sensors towards 100 ppm and 40000 ppm H_2 gas in N_2 at 25–250 °C after treatment at 250 °C, i.e. after the formation of InPd IMC in PdO/rh-In_2O_3 sample.

free atmospheres at low temperatures on metal oxides can be attributed to the hydrogen ionosorption, at higher temperatures - to surface hydroxylation; both processes result in an increase of charge carrier density in the semiconducting material (indium oxide). Surface hydroxylation has been reported for several metal-oxide semiconductors, such as ZnO and SnO_2.[16,17] For example, Grossman has observed H–O bond formation on the SnO_2 surface exposed to H_2 gas, using operando diffuse reflectance infrared Fourier transform (DRIFT) spectroscopy.[16,18] It was suggested that dissociated H adatoms on SnO_2 are bound to lattice oxygen atoms and form hydroxyl surface groups that act as electron donors.[19]

Both experimental works and *ab initio* calculations[20,21,22] have demonstrated that In_2O_3 (an intrinsic n-type semiconductor) is able to sustain dissociative hydrogen adsorption with further entrapping hydrogen, where both interstitial and substitutional hydrogen atoms act as shallow carrier donors.[23]

The barrier for dissociation of H_2 molecule on the pristine c-In_2O_3 surface was calculated to be ~0.85 eV, and oxygen vacancies cause a slight reduction of this barrier. Furthermore, such adsorption might result in In_2O_3 surface hydroxylation and water molecule formation, which desorb and leave oxygen vacancies.[20,22] All these processes increase the charge carrier density in the system and thus decrease the resistance of the sensor, which was observed in the gas sensing tests. However, as we can see, the sensitivity of the pure rhombohedral indium oxide sensor to hydrogen is negligible at low temperatures (below 100 °C) and becomes to be noticeable only at temperatures above 100 °C. For PdO, which is a p-type semiconductor, with Eg = 2.2 eV,[24] the sensing process is more complicated.

First, PdO is reduced to Pd during exposure to hydrogen[25] at temperatures far lower than 100 °C,[12] and according to this and another study,[26] even at highly diluted hydrogen concentrations (6000 ppm and below). Thus, as demonstrated by XRD and XPS PdO particles are partially reduced to Pd onto the PdO core during exposure to hydrogen gas at 25 °C. Metallic palladium is another catalyst that promotes H_2 dissociation[22] but at much lower temperatures in comparison to pure rh-In_2O_3, and leads to the atomic hydrogen spillover[27] from Pd particles onto the In_2O_3 surface, followed by its ionosorption and surface hydroxylation[28] (where hydrogen can connect even on vacant oxygen lattice sites[28,29]). These processes could increase electron concentration in the conduction band of the sensor, decreasing its resistance. Moreover, palladium is well known for its high ability to dissolve hydrogen in vast quantities, forming palladium hydride PdH_x ($x < 1$) at low temperatures (50–120 °C).[30] The palladium-hydrogen interaction is one of the most studied systems because the high specific solubility of hydrogen in palladium is widely used in several industrial processes, for instance, in membranes for hydrogen purification and hydrogen storage systems. As for electrical properties, during the adsorption of H_2 molecules, hydride formation occurs, and the metallic conductivity falls until a composition of around $PdH_{0.5}$ is reached, at which point the solid becomes a semiconductor.[31] As dissolved hydrogen atoms also cause an increased scattering of conducting electrons, there is a corresponding decrease in the conductivity of α-PdH_x; this effect is the basis of palladium-based resistive gas sensors (chemiresistors). Because of the relatively low miscibility gap, hydrogen has a maximum solubility in a hydrogen-poor α-PdH_x (x_{max} of around 0.01 for bulk α-PdH_x). Above this concentration, a phase transformation occurs above a H/Pd ratio of 0.01 with the formation of the so-called β-phase where the lattice parameter drastically increases from around 3.90 to around 4.04 Å. This transition was not observed in our work.

As demonstrated above, the PdO/rh-In_2O_3 sensor shows a high response even for 100 ppm H_2 gas at temperatures around 40 °C where PdO is completely reduced to metallic Pd, and the dissociation/ionosorption processes reach their maximum effectiveness at the temperature range of 70–100 °C. Starting from around 150 °C, the desorption process is getting stronger, and the overall response values start to decrease. The next fast drop of the response is observed after 250 °C, where In_2O_3 and Pd start to form InPd IMC, which does not adsorb hydrogen[32] and hence, reduces the number of catalytic adsorption sites on the surface of the sensor.

Conclusion

In the present work, the correlation between structure and gas sensing properties of the PdO/rh-In_2O_3 system has been studied by complementary resistance measurements with synchrotron-based in situ X-ray diffraction (XRD) and ex situ X-ray photoelectron spectroscopy (XPS). The results of the in situ XRD and ex situ XPS experiments reveal that PdO/rh-In_2O_3 undergoes a sequence of phase transformations with temperature under diluted H_2 gas similar to that observed during the treatment in the pure H_2 atmosphere. Gas tests conducted with pure rh-In_2O_3 have shown a huge difference in the R_{N2}/R_{H2} ratio in comparison to PdO-loaded rh-In_2O_3, suggesting that Pd catalyzes dissociation, spillover, and adsorption of hydrogen at a much lower temperature (~70 °C and below) than the pure rh-In_2O_3. The outstanding response of PdO/rh-In_2O_3 sensors towards H_2 in the temperature range 25–150 °C is due to the catalytic dissociation of H_2 on palladium. The response of the sensor is significantly decreased after 250 °C due to the formation of intermetallic compounds such as InPd (which do not adsorb hydrogen) together with higher desorption rates. The formation of the InPd IMC leads to a significant diminishing of the hydrogen adsorption capability and a reduction of the spillover effect.

Experimental Section

Materials: The preparation of the specimens used in this work has been described previously.[12] Briefly, pure metastable nanoscaled rh-In_2O_3 was produced by calcination of indium oxyhydroxide (InOOH) at >375 °C in an ambient atmosphere according to the methodology developed recently.[33] The loading of 5 wt% of nanoscaled PdO onto rh-In_2O_3 powder was achieved by incipient wetness impregnation method where $Pd(NO_3)_2 \cdot 2H_2O$ (Sigma Aldrich) was dissolved in deionized water, and the latter solution was added dropwise to the vigorously stirred rh-In_2O_3 suspension in deionized water. The preparation is finished by calcination of the material in the air at 300 °C for 30 min, resulting in PdO/rh-In_2O_3 powder which consists of spherical grains with typical sizes ranging between 30 and 50 nm.

In Situ Synchrotron X-ray Diffraction (XRD) was performed at beamline 12.2.2 at the Advanced Light Source (ALS, Berkeley, USA) with a monochromatic beam energy of 25 keV ($\lambda = 0.49649$ Å) and a spot size of $30 \times 30\ \mu m^2$. About 1 mg of powder form material was placed in quartz capillaries (Hilgenberg GmbH, Germany) with outer diameters of 700 μm, with gas injection accomplished using a concentrical inner 500 μm capillary with cut-open ends. Heating, as well as cooling rates, realized in a low-power infrared tube furnace,[34] were chosen as 20 $Kmin^{-1}$ for all experiments. A Perkin Elmer flat panel detector (XRD 1621, with dark image and strain correction) was used to record the XRD patterns every 25 s. Rietveld refinement and Le Bail fits was performed using FULLPROF software[35] using the Thompson-Cox-Hastings pseudo-Voigt function convoluted with axial divergence asymmetry. The resolution function of the instruments was determined from the structure refinement of the standard material LaB_6.

X-ray Photoelectron Spectroscopy (XPS) measurements were performed on the samples after gas sensing tests using the K-Alpha photoelectron spectrometer (Thermo Fisher Scientific, USA) equipped with a monochromatic Al Ka source. Scans were recorded in the constant analyzer energy mode with a pass energy of 50 eV, step size of 0.1 eV, and a spot size of 400 μm. Deconvolution of the spectra was performed using XPS41 software using the Lorentzian-Gaussian function.

The morphology and elemental compositions of the fabricated sensors were examined by **Scanning Electron Microscopy (SEM)** in a Zeiss Leo 1530 Gemini (Germany) coupled with an energy dispersive X-ray detector (Thermo Fisher Scientific, USA). The aperture of the SEM detector was set to 30 μm, and 120 μm for the EDX. The SEM measurements were executed at an energy of 5 kV, and EDX at an energy of 10 kV at the Helmholtz Zentrum Berlin (HZB).

Fabrication of Gas Sensors and Gas Sensing Tests: rh-In_2O_3 and PdO/rh-In_2O_3 gas sensors were fabricated by dropping corresponding suspensions on sensor substrates (polycrystalline alumina with Pt electrodes on the front side and Pt resistive heater on the backside, Figure S1). The suspensions were prepared by dispersing a few mg of the sample powder in pure ethanol (Sigma Aldrich) upon ultrasonication (Bandelin Sonorex Super RK 100). The deposited materials were dried at room temperature for several hours to evaporate the leftovers of ethanol from the prepared coating. Gas tests have been conducted using a home-build setup (Figure S1a). Target gases (4 vol% H_2 in 96 vol% N_2, Air Liquide) were diluted in N_2 (Air Liquide, 99.999 % purity), and the flow rates were precisely controlled by a set of mass flow controllers (Bronkhorst EL-Flow Prestige Series) to obtain desired gas concentrations. The total flow rate was kept constant at 150 ml/min. The resistance signals of the studied sensors were measured by a set of multimeters (Tektronix DMM 4050 and Keithley DMM 7510) with auto range and filter off, and the sampling rate was set to 1 Hz. Power sources (Manson SSP-8160 and Keysight U8001A) were connected to heater (back-side) electrodes for resistive sensor heating. Most of the equipment was connected to a computer and programmed with the LabVIEW software. The gas test program was set as follows. First, the sensors are purged for 10 hours with pure N_2 flow to stabilize the sensor resistance followed by 1 hour of consequent H_2 concentrations (100 ppm, 200 ppm, 500 ppm, 1000 ppm, 5000 ppm, 10,000 ppm, and 40000 ppm). Finally, sensors were purged with pure N_2 for 10 hours. (Figure S2). This test program was repeated at different temperatures (25–450 °C) to monitor the real-time resistance change of the samples during H_2 gas sensing. The sensor signals are calculated as the ratio R_{N2}/R_{H2}, where R_{N2} is the sensors resistance in nitrogen (in the absence of the hydrogen), R_{H2} – the sensor resistance in the presence of the defined H_2 concentration in the nitrogen.

Author Contributions

O.O.: Conceptualization, Methodology, Formal analysis, Investigation, Validation, Data Curation, Visualization, Writing – Original Draft; **M. F. B.**: Conceptualization, Formal analysis, Investigation, Data Curation, Validation, Writing – Review & Editing, Supervision; **A.G.**: Investigation, Writing – Review & Editing; **A.G.**: Conceptualization, Writing – Review & Editing, Supervision, Project administration, Funding acquisition.

Acknowledgements

We want to thank Dr. Oliver Görke and Fabian Zemke for their help with the SEM & EDX measurements; Franz Kamutzki, Lukas Schlicker, and Benjamin Bischoff for their help with the in situ XRD measurements; Dipl.-Ing. Kai Weisser and Dipl.-Ing. Delf Kober for the help with establishing the gas sensing setup. The authors thank the Advanced Light Source, which is supported by the Director, Office of Science, Office of Basic Energy Sciences, of the U.S. Department of Energy under Contract No. DE-AC02-05CH11231, and where the in situ XRD measurements were conducted at beamline 12.2.2 in the framework of the proposals AP (ALS-08408) and GUP (ALS-10533). Open Access funding enabled and organized by Projekt DEAL.

Conflict of Interest

The authors declare no conflict of interest.

Data Availability Statement

The data that support the findings of this study are available from the corresponding author upon reasonable request.

Keywords: indium oxide · palladium · in situ X-ray diffraction · gas sensors · hydrogen

[1] T. van Nguyen, V. C. Nguyen, D. van Nguyen, S. H. Hoang, N. Hugo, D. H. Nguyen, H. van Nguyen, *J. Hazard. Mater.* **2016**, *301*, 433–442.
[2] Q. A. Drmosh, Z. H. Yamani, *Ceram. Int.* **2016**, *42*, 12378–12384.
[3] C. Zhang, A. Boudiba, M.-G. Olivier, R. Snyders, M. Debliquy, *Sens. Actuators B* **2012**, *175*, 53–59.
[4] S. Joo, I. Muto, N. Hara, *J. Electrochem. Soc.* **2010**, *157*, 221–226.
[5] M. Pashchanka, R. C. Hoffmann, A. Gurlo, J. J. Schneider, *J. Mater. Chem.* **2010**, *20*, 8311–8319.
[6] K. Hassan, A. I. Uddin, F. Ullah, Y. S. Kim, G.-S. Chung, *Mater. Lett.* **2016**, *176*, 232–236.
[7] A. Gurlo, D. R. Clarke, *Angew. Chem. Int. Ed. Engl.* **2011**, *50*, 10130–10132.
[8] Y.-S. Shim, L. Zhang, D. H. Kim, Y. H. Kim, Y. R. Choi, S. H. Nahm, C.-Y. Kang, W. Lee, H. W. Jang, *Sens. Actuators B* **2014**, *198*, 294–301.
[9] D. Zhang, Y. Sun, C. Jiang, Y. Zhang, *Sens. Actuators B* **2017**, *242*, 15–24.
[10] S. A. Müller, D. Degler, C. Feldmann, M. Türk, R. Moos, K. Fink, F. Studt, D. Gerthsen, N. Bârsan, J.-D. Grunwaldt, *ChemCatChem* **2018**, *10*, 864–880.
[11] A. Gurlo, P. Kroll, R. Riedel, *Chem. Eur. J.* **2008**, *14*, 3306–3310.
[12] L. Schlicker, M. F. Bekheet, A. Gili, A. Doran, A. Gurlo, K. Ploner, T. Schachinger, S. Penner, *J. Solid State Chem.* **2018**, *266*, 93–99.
[13] a) M. Brun, A. Berthet, J. Bertolini, *J. Electron Spectrosc. Relat. Phenom.* **1999**, *104*, 55–60; b) M. C. Militello, S. J. Simko, *Surf. Sci. Spectra* **1994**, *3*, 387–394; c) S. Sinha, S. Badrinarayanan, A. P. B. Sinha, *J. Phys. F: Met. Phys.* **1986**, *16*, L229–L232.
[14] G. M. McGuirk, J. Ledieu, É. Gaudry, M.-C. de Weerd, V. Fournée, *J. Chem. Phys.* **2014**, *141*, 84702.
[15] M. Neumann, D. Teschner, A. Knop-Gericke, W. Reschetilowski, M. Armbrüster, *J. Catal.* **2016**, *340*, 49–59.
[16] K. Grossmann, R. G. Pavelko, N. Barsan, U. Weimar, *Sens. Actuators B* **2012**, *166–167*, 787–793.
[17] C. G. van de Walle, *Phys. Rev. Lett.* **2000**, *85*, 1012–1015.
[18] K. Großmann, S. Wicker, U. Weimar, N. Barsan, *Phys. Chem. Chem. Phys.* **2013**, *15*, 19151–19158.
[19] M. Hübner, R. G. Pavelko, N. Barsan, U. Weimar, *Sens. Actuators B* **2011**, *154*, 264–269.
[20] A. Posada-Borbón, H. Grönbeck, *Phys. Chem. Chem. Phys.* **2020**, *22*, 16193–16202.
[21] a) D. Albani, M. Capdevila-Cortada, G. Vilé, S. Mitchell, O. Martin, N. López, J. Pérez-Ramírez, *Angew. Chem. Int. Ed. Engl.* **2017**, *56*, 10755–10760; b) M. S. Frei, M. Capdevila-Cortada, R. García-Muelas, C. Mondelli, N. López, J. A. Stewart, D. Curulla Ferré, J. Pérez-Ramírez, *J. Catal.* **2018**, *361*, 313–321.
[22] M. S. Frei, C. Mondelli, R. García-Muelas, K. S. Kley, B. Puértolas, N. López, O. V. Safonova, J. A. Stewart, D. Curulla Ferré, J. Pérez-Ramírez, *Nat. Commun.* **2019**, *10*, 3377.
[23] a) S. Limpijumnong, P. Reunchan, A. Janotti, C. G. van de Walle, *Phys. Rev. B* **2009**, *80*, 193202; b) T. Koida, H. Fujiwara, M. Kondo, *Jpn. J. Appl. Phys.* **2007**, *46*, L685–L687; c) P. D. C. King, R. L. Lichti, Y. G. Celebi, J. M. Gil, R. C. Vilão, H. V. Alberto, J. Piroto Duarte, D. J. Payne, R. G. Egdell, I. McKenzie, C. F. McConville, S. F. J. Cox, T. D. Veal, *Phys. Rev. B* **2009**, *80*, 081201; d) W. Yin, K. Smithe, P. Weiser, M. Stavola, W. B. Fowler, L. Boatner, S. J. Pearton, D. C. Hays, S. G. Koch, *Phys. Rev. B* **2015**, *91*, 075208.
[24] S. V. Ryabtsev, V. M. Ievlev, A. M. Samoylov, S. B. Kuschev, S. A. Soldatenko, *Thin Solid Films* **2017**, *636*, 751–759.
[25] Y. Shen, T. Yamazaki, Z. Liu, D. Meng, T. Kikuta, N. Nakatani, M. Saito, M. Mori, *Sens. Actuators B* **2009**, *135*, 524–529.
[26] Y.-J. Chiang, K.-C. Li, Y.-C. Lin, F.-M. Pan, *Phys. Chem. Chem. Phys.* **2015**, *17*, 3039–3049.
[27] a) S. J. Teichner, *Appl. Catal.* **1990**, *62*, 1–10; b) U. Roland, F. Roessner, *Stud. Surf. Sci. Catal.* **1997**, *112*, 191–200.
[28] T. Bielz, H. Lorenz, W. Jochum, R. Kaindl, F. Klauser, B. Klötzer, S. Penner, *J. Phys. Chem. C* **2010**, *114*, 9022–9029.
[29] A. Samanta, J. B. Varley, V. Lordi, *Appl. Phys. Lett.* **2020**, *117*, 62103.
[30] F. D. Manchester, A. San-Martin, J. M. Pitre, *JPE* **1994**, *15*, 62–83.
[31] N. N. Greenwood, A. Earnshaw, *Chemistry of the elements*, Butterworth-Heinemann, Oxford **1997**, p. 1151.
[32] M. Wencka, M. Hahne, A. Kocjan, S. Vrtnik, P. Koželj, D. Korže, Z. Jagličić, M. Sorić, P. Popčević, J. Ivkov, A. Smontara, P. Gille, S. Jurga, P. Tomeš, S.

Paschen, A. Ormeci, M. Armbrüster, Yu. Grin, J. Dolinšek, *Intermetallics* **2014**, *55*, 56–65.

[33] a) L. Schlicker, M. F. Bekheet, A. Gurlo, *Z. Kristallogr. Cryst. Mater.* **2017**, *232*, 129–140; b) L. Schlicker, R. Popescu, M. F. Bekheet, A. Doran, D. Gerthsen, A. Gurlo, *Nanoscale* **2019**, *11*, 12242–12249.

[34] a) A. Doran, L. Schlicker, C. M. Beavers, S. Bhat, M. F. Bekheet, A. Gurlo, *Rev. Sci. Instrum.* **2017**, *88*, 13903; b) L. Schlicker, A. Doran, P. Schneppmüller, A. Gili, M. Czasny, S. Penner, A. Gurlo, *Rev. Sci. Instrum.* **2018**, *89*, 33904.

[35] J. Rodríguez-Carvajal, *IUCr Newsletter* **2001**, *26*, 12–19.

Manuscript received: October 17, 2022
Revised manuscript received: February 13, 2023
Accepted manuscript online: February 20, 2023
Version of record online: March 6, 2023